ELSEVIER

Journal of Electron Spectroscopy and Related Phenomena 100 (1999) 119–135

JOURNAL OF ELECTRON SPECTROSCOPY and Related Phenomena

www.elsevier.nl/locate/elspec

NEXAFS spectromicroscopy of polymers: overview and quantitative analysis of polyurethane polymers

Stephen G. Urquhart[a], Adam P. Hitchcock[b,*], Archie P. Smith[a], Harald W. Ade[a], Werner Lidy[c], Ed G. Rightor[c], Gary E. Mitchell[c]

[a]*Department of Physics, North Carolina State University, Raleigh, NC 27695-8202, USA*
[b]*Brockhouse Institute for Materials Research, McMaster University, Hamilton, ONT, Canada L8S 4M1*
[c]*Dow Chemical USA, Midland, MI 48667, USA*

Received 4 January 1999; accepted 19 April 1999

Abstract

The successful application of X-ray spectromicroscopy to chemical analysis of polymers is reviewed and a detailed application to quantitative analysis of polyurethanes is presented. Near Edge X-ray Absorption Fine Structure (NEXAFS) spectroscopy is the basis of chemical sensitive X-ray imaging, as well as qualitative and quantitative micro-spectroscopy. These capabilities are demonstrated by a review of recent work, and by presentation of new results outlining a methodology for quantitative speciation of polyurethane polymers. C 1s inner-shell excitation spectra of a series of molecular and polymeric model compounds, recorded by gas phase inelastic electron scattering (ISEELS) and solid phase NEXAFS techniques, are used to understand the spectroscopic basis for chemical analysis of polyurethanes. These model species contain the aromatic urea, aromatic urethane (carbamate) and aliphatic ether functionalities that are the main constituents of polyurethane polymers. Ab initio calculations of several of the model molecular compounds are used to support spectral assignments and give insight into the origin and relative intensities of characteristic spectral features. The model polymer spectra provide reference standards for qualitative identification and quantitative analysis of polyurethane polymers. The chemical compositions of three polyurethane test polymers with systematic variation in urea/urethane content are measured using the spectra of model toluene diisocyanate (TDI) urea, TDI-carbamate, and poly(propylene oxide) polymers as reference standards.

Keywords: NEXAFS microscopy; Polyurethanes; Molecular models; Polymer quantitative analysis

1. Introduction

Inner-shell excitation of molecules and solids can be studied by either inelastic electron scattering (Inner Shell Electron Energy Loss Spectroscopy, ISEELS) [1,2] or Near Edge X-ray Absorption Fine Structure (NEXAFS) [3]. Recently there has been considerable activity in developing inner-shell excitation spectroscopy as a high spatial resolution analytical technique, as in NEXAFS X-ray microscopy [4–12] or Electron Energy Loss Spectroscopy (EELS) in a transmission electron microscope [13,14]. In this form, inner-shell excitation spectroscopy provides a useful tool for the microanalysis of many types of materials including polymers.

*Corresponding author.
E-mail address: aph@mcmaster.ca (A.P. Hitchcock)

0368-2048/99/$ – see front matter
PII: S0368-2048(99)00043-2

However, for maximum analytical utility it is important to have spectra of compounds of known structure for fingerprint purposes. In most cases, it is also very helpful to have detailed spectroscopic assignments based on comparisons of series of closely related chemical species, aided by the results of high-quality quantum chemical calculations [15–18]. This article briefly reviews X-ray spectromicroscopy and its applications to polymer microanalysis. We subsequently document the power of NEXAFS spectroscopy by demonstrating quantitative speciation of polyurethane polymers. We emphasize the use of co-ordinated, complementary ISEELS and NEXAFS studies of model compounds to assist the analysis of the spectra of these complex polymers. The chemical analysis capability is exemplified by the use of NEXAFS spectroscopy for the quantitative compositional analysis of urea and urethane linkages in polyurethane polymers. In this work, we deal exclusively with the spectroscopic basis for the speciation and its application to homogeneous model polymers; demonstration of speciation on a submicron spatial scale by NEXAFS spectromicroscopy is presented elsewhere [19,20].

Polyurethanes are complex materials that may consist of a variety of component species, depending on both the reagents and conditions of polymerization [21]. Polyurethanes are formed from three primary components: diisocyanate monomer, multifunctional polyether-polyols, and water. For many applications the diisocyanate is an aromatic compound – typically either toluene diisocyanate (mixed 2,4 and 2,6 isomers) (TDI) or 4,4′ methylene bis(phenyl isocyanate) (MDI). Two linkages are the primary building blocks of the polyurethane backbone: urethane (carbamate) and urea. Urethane linkages are formed by the one step reaction of an isocyanate group with the OH group of a polyether-polyol. Urea linkages are the outcome of a two step reaction of two isocyanate groups and water, where CO_2 gas is evolved.

The spectra of model polymers are used to provide reference standards for the quantitative analysis (‘speciation’) of polyurethane polymers. We began the exploration of the use of core excitation for quantitative analysis a number of years ago by demonstrating that both EELS [22,23] and NEXAFS [24] are able to distinguish and quantify the amounts of aromatic and aliphatic components of polyurethanes. Here we explore how the spectra of model polymers can be used as standards for quantitation of the three principle components of a complex polyurethane (ether, urea, and urethane). Quantitative, spatially resolved analysis of functional group composition (particularly the urea and urethane content) is needed to help understand the chemical basis for the microstructure of polyurethane polymers [21,25,26]. Such information can be correlated with physical and mechanical properties and then be used to optimize formulation chemistry [21].

This paper is organized as follows. Section 2 provides a brief description of the current status of soft X-ray spectromicroscopy, as it applies to polymers. An example of its application to poly(ethylene terephthalate)/Vectra™ blends [27] is given in some detail. Section 3 uses a sample STXM micrograph to motivate the work on quantitative compositional analysis of polyurethane polymers. It then presents the spectroscopic basis for speciation of the principle components of polyurethanes, based on experimental studies (Section 3.1) and ab initio calculations (Section 3.2) of model molecules, and STXM studies of single component polymer model compounds (Section 3.3). Section 4 then applies this knowledge to quantitative speciation of three model polyurethanes, custom synthesized to test the quantitation capabilities of NEXAFS spectroscopy. All spectra of model single and multiple component polymers were obtained using either the NSLS or ALS scanning transmission X-ray microscopes (STXM) in order to have a proper evaluation of these NEXAFS microscopes for the desired quantitation, under conditions identical to that used to study heterogeneous polymer samples [19,20].

2. Current status of X-ray spectromicroscopy of polymers

Spectromicroscopy refers to the combined use of selective energy imaging and spectroscopy at high spatial resolution. It is an integration of the spectroscopic and imaging aspects of analytical microscopy. Synchrotron-based X-ray microscopy in various implementations is an excellent example of spectromicroscopy. There are X-ray microscopes in both the

soft X-ray (<1500 eV) and hard X-ray regimes (>1500 eV) at many of the world's synchrotrons. Initial developments in zone plate based X-ray microscopy focused on biological applications [5]. More recently, the potential for powerful and often unique applications in material science and molecular environmental science has become appreciated. The lower radiation damage [28], excellent chemical sensitivity [4,10], and ability to examine solvated materials [29–31] are some of the strengths relative to electron microscopy techniques. At present, the prospects for significant contributions by X-ray microscopy to polymer science and technology are excellent. The number of X-ray microscopes has been growing rapidly in the last few years, with new microscopes coming on-line at the Advanced Light Source (ALS) in Berkeley [11,12] and other third generation synchrotron radiation facilities worldwide.

Volume 84 of this journal was a special issue that gave a comprehensive overview of all types of soft X-ray spectromicroscopy. Here we focus our discussion on scanning transmission X-ray microscopy (STXM), as it is this type of instrument that has been used most extensively for polymer research. STXM is preferred for high energy resolution NEXAFS microscopy of polymers because radiation damage rates are reduced relative to Transmission X-ray Microscopy (TXM) (no low efficiency optical elements after the sample), and because current generation STXM microscopes can perform both microspectroscopy and energy selective imaging at higher energy resolution than presently existing full-field imaging soft X-ray microscopes (TXM).

A schematic of a STXM beamline is presented in Fig. 1. The Stony Brook STXM at the National Synchrotron Light Source (NSLS) [10] and the BL7.0.1 STXM at the ALS [11,12] use undulators as the X-ray source. Undulators are several orders of magnitude brighter than bending magnet sources and about eight to ten orders of magnitude brighter than non-tunable laboratory X-ray tubes. In a STXM, monochromated X-rays are focussed by a Fresnel zone plate, which is a circular, variable line density, transmission diffraction grating. A central stop in the zone plate, in conjunction with a slightly smaller order sorting aperture (OSA), is used to isolate the positive first order diffraction and to suppress unwanted diffraction orders. In most instruments the sample is mechanically raster scanned in the focal plane of the spot, although one zone plate based X-ray microscope has recently been implemented in which an over-filled zone plate rather than the sample is raster scanned [12]. The spot size achieved with the zone plate determines the spatial resolution of the microscope, which is about 40 nm with the best quality zone plates currently available. The sample is located in an air or He atmosphere and is investigated at room temperature.

In addition to imaging, the focused beam can be left on the same spot while the photon energy is scanned. Absorption spectra (optical density, OD) are then derived from the transmitted X-ray intensity as $(-\ln(I/I_0))$, where an energy scan from the sample

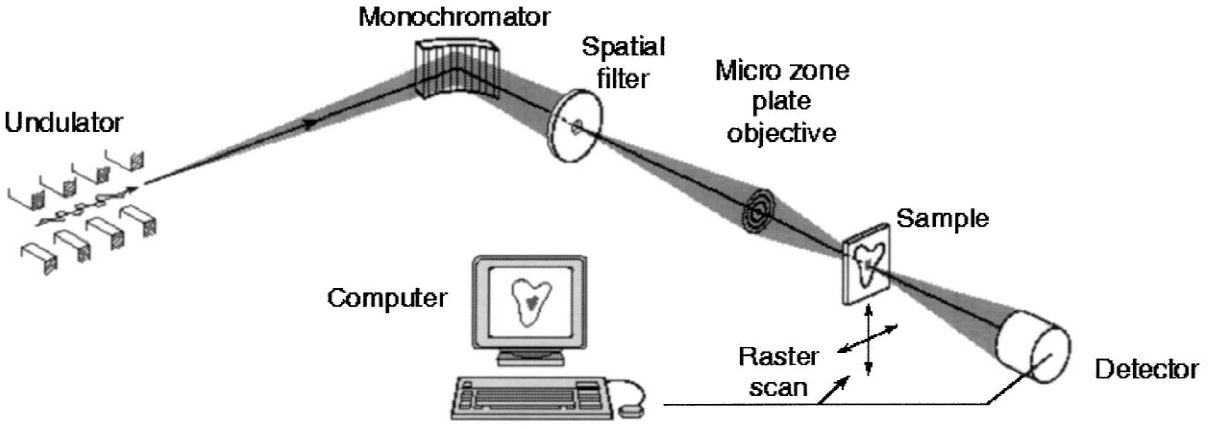

Fig. 1. Schematic of a scanning transmission X-ray microscope.

(I) is normalized to another energy scan recorded without a sample (I_0). Quantitative analysis is provided by the Beer's law dependence of the absorbance:

$$A = OD = \mu\rho t = -\ln(I/I_0)$$

where μ is the energy dependent mass absorption coefficient, ρ is the density, and t is the sample thickness. Spectra are acquired with resolving powers of 2000–9000, corresponding to an energy resolution in the C 1s region of about 0.2 eV at NSLS and better than 0.1 eV at the ALS. In principle, all elements with inner shell thresholds in the 150–1200 eV energy range can be accessed with NEXAFS microscopy, although most work to date has used the carbon 1s edge. At this core edge, energy calibration is provided in situ by leaking CO_2 into the microscope atmosphere while the sample is in place [10].

Typically, polymer sections ~100 nm in thickness are optimum for carbon K-edge NEXAFS. Samples much thinner than 80 nm often suffer rapid beam damage and their spectra have a poor signal to noise ratio whereas the spectra of samples much thicker than 200 nm can be distorted by absorption saturation. Spectroscopy of thicker samples is a particular problem when the beam is contaminated by higher order photons or if the X-ray detector has appreciable dark noise. This effect causes an attenuation of strongly absorbing features. If required, spectra can be normalized for thickness and density variations between different sample locations by utilizing the high energy continuum cross-section (>320 eV for C 1s NEXAFS) where the signal is only sensitive to elemental composition. Similarly, density and thickness variations in images can be detected and corrected for by acquiring an image above 320 eV, or by isolating the chemical composition information via ratios of images.

In principle, the spatial resolution of NEXAFS microscopy is much lower than that obtained with transmission electron microscopy (TEM). However, in practice, the need for a high dose to acquire useful core excitation spectra by electron energy loss spectroscopy (EELS), combined with the low critical dose for radiation damage of most polymers, means that the effective spatial resolution that can be achieved for *analytical* measurements is often comparable [28]. While radiation damage rates are considerably lower in soft X-ray spectroscopy than in TEM–EELS [28], radiation damage is still of some concern, particularly when high quality spectra are acquired from small sample areas or the sample is particularly radiation sensitive. Acquiring spectra indirectly through a sequence of images ('stacks' [32]) or linescans, can offer considerable advantages in such cases, since image acquisition generally requires lower dose per pixel than point spectra. A STXM capable of examining samples at cryogenic temperatures has recently been implemented at NSLS [33]. Cooling the sample is known to reduce the rate of radiation damage in TEM of polymers. A similar beneficial effect is expected when cryo-STXM techniques are applied to polymers.

Many polymer systems and problems have already been investigated with NEXAFS microscopy. These include studies of: morphology of poly(ethylene terphthalate)–polycarbonate (PET/PC) blends without staining [8]; morphology and composition of PET–oxybenzoate/oxynapthoate (Vectra™) blends [27], rubber toughened poly(methyl methacrylate) (PMMA) [34,35], and macrophase-separated random block copolymer/homopolymer blends [36]; orientation of molecular chains in Kevlar [7,9] and on rubbed polyimide surfaces [37]; chemical changes inside wear tracks in lubrication layers on hard disks [38,39]; dewetting and phase separation kinetics in polymer thin films [40–42]; characterization of phase separation during processing, such as precipitates in polyurethanes [4,43] and multi-phase liquid crystalline polyesters [44]; chemical mechanism of fire-resistance imparted to heat treated polyacrylonitrile fibers [45]; development of exposure strategies for poly(methyl methacrylate) resists [46]; variation of cross-linking in non-uniformly cross-linked hydrated polymers [29,30]; micro-emulsions in thin polymer films [31]; as well as studies of biological [5,47] and organic geochemical [48–51] samples. Several reviews, which describe details and provide images and spectra from most of these applications, have been published relatively recently [4,52].

2.1. NEXAFS microscopy of poly(ethylene terephthalate)/Vectra™ blends

Here, we exemplify the power of NEXAFS microscopy with a recent application that allowed us to

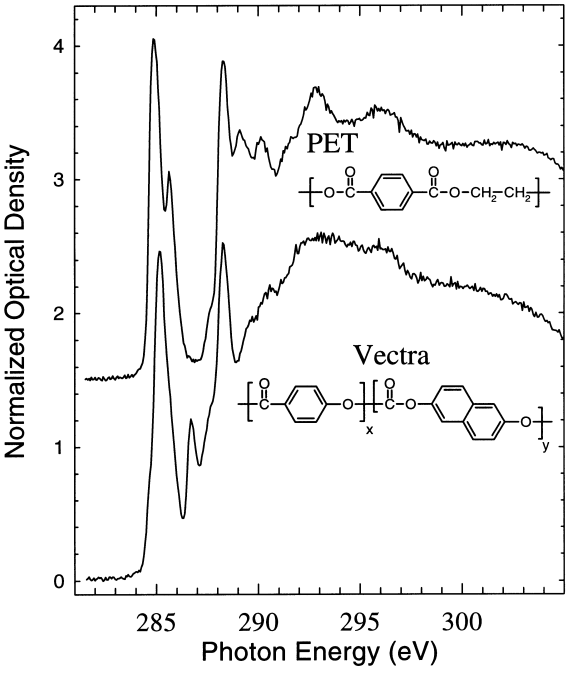

Fig. 2. NEXAFS reference spectra of poly(ethylene terephthalate) (PET) and Vectra™, shown with their respective chemical structures ($x=0.73$ and $y=0.27$ for Vectra™). Differences in the relative X-ray absorption of these materials (at, e.g. 286.7 eV) were exploited in order to discern the morphologies of mechanically alloyed blends of PET and Vectra™ (see Figs. 3 and 4).

delineate the morphology in blends of poly(ethylene terephthalate) (PET) and Vectra™ A950, (73/27 mol% oxybenzoate/2,6-oxynaphthoate) produced by mechanical alloying [27]. No preferential, heavy metal stain exists for enhancing the contrast between these two polymers in Electron Microscopy and spectroscopic means had to be utilized to differentiate and quantitate these two components. Fig. 2 shows the reference spectra of these polymers. Although relatively similar functional groups are present, the NEXAFS spectra are quite different, and NEXAFS microscopy had little difficulty delineating the morphology in these materials. The example shown in Fig. 3 is from blends that were produced by mechanical alloying at −180°C and subsequent melt-pressing into films at 285°C. It was observed that these blends retain much of the degree of mixing imparted by alloying after post-processing in the molten state, and that the Vectra™ dispersions contain little, if any PET. Molecular orientation of the Vectra™, a liquid crystalline polymer, was investigated with linear dichroism. Anisotropic orientation of the Vectra™ molecules was only observed in domains larger than 2 μm (see Fig. 4).

3. X-ray microscopy of polyurethane polymers: motivation for speciation

Depending on the formulation and processing, many polyurethanes exhibit macrophase separation with feature sizes larger than 100 nm [21]. A sample STXM micrograph of such a polyurethane polymer is presented in Fig. 5. This image was recorded at 285 eV with the NSLS STXM using 4 ms per pixel. At the ALS images of similar statistical quality but slightly worse spatial resolution are obtained using a sub-micron pixel dwell on account of the higher source brightness and thus larger coherent flux through the zone plate. The sample imaged in Fig. 5

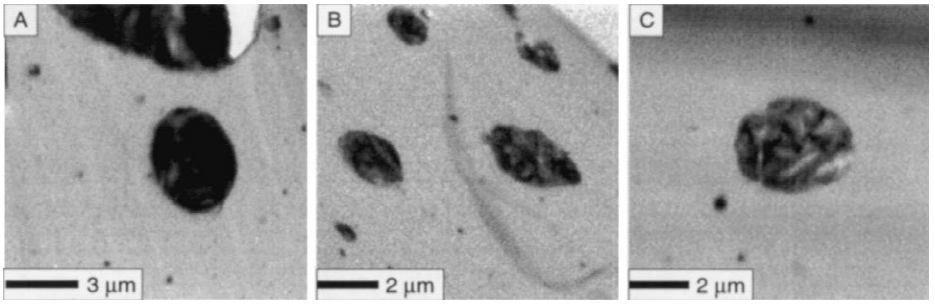

Fig. 3. STXM images acquired at 286.7 eV of PET/Vectra™ blends differing in composition (in w/w PET/Vectra™): (A) 75/25, (B) 90/10 and (C) 99/1. High image contrast allowed easy assessment of the size distribution of Vectra™ dispersions within the PET matrix. The internal structure of the Vectra™ domains is primarily due to molecular orientation (see Fig. 4).

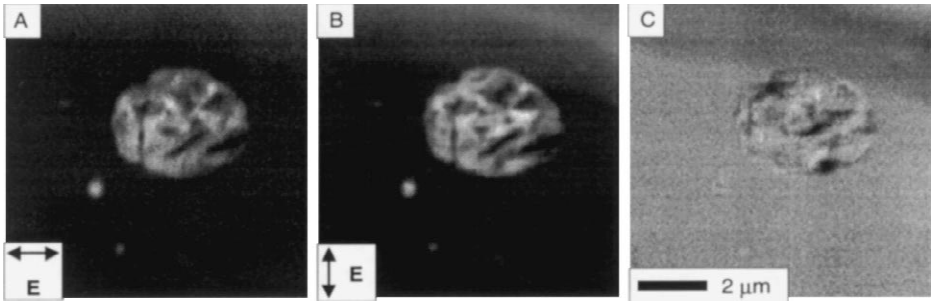

Fig. 4. STXM images acquired at 286.7 eV of a 99/1 w/w PET/Vectra™M blend subjected to post-milling melt pressing. Images (A) and (B) have been converted to optical density which is why the contrast appears reversed to the images in Fig. 3. In images (A) and (B), the electric polarization vector ($\hat{E}$) is rotated by 90° with respect to each other, as indicated. Differences in intensity in these images are primarily due to anisotropic molecular orientation. The ratio of these images (C) reveals the linear dichroism of the specimen. Small Vectra™ domains appear gray and possess no discernible orientation, whereas the large dispersion exhibits a measurable degree of molecular orientation (black and white areas) due to the nematic nature of this liquid crystalline polymer.

is a thin section of a high water, TDI-based polyurethane plaque. TEM micrographs of high water polyurethanes exhibit a similar appearance. TEM results, along with analytical results from other sample characterization techniques, have been presented elsewhere [25,26]. The strong contrast at 285 eV is reflective of the high aromatic content of the precipitates in this high water polyurethane. Our objective in studying these polyurethane polymers is to quantify and map the composition, in particular the urea and urethane content, and possibly that of minority species, in a variety of formulations and thereby determine relationships between chemical composition, processing, and properties of the final polymer product. The ultimate goal of the quantitative analysis methodology is to be able to determine the functional group composition at the instrumental resolution in an image like that in Fig. 5.

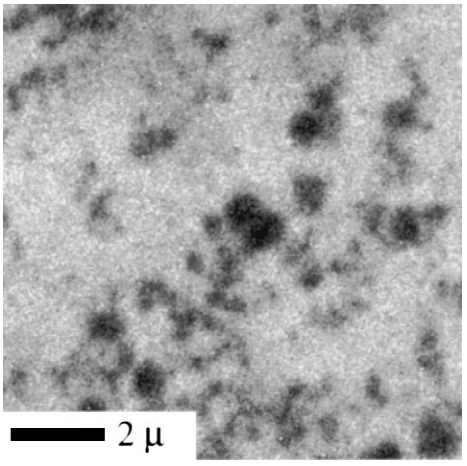

Fig. 5. STXM image of a high-water, TDI-based polyurethane recorded at 285 eV with the NSLS STXM using 4 ms per pixel. The dark areas are aromatic-rich hard segments, while the uniform matrix is enriched in the aliphatic polyether component. The ultimate goal of the quantitative analysis methodology is to determine the functional group composition at each pixel in this type of image.

3.1. Molecular model studies by ISEELS spectroscopy

While there is considerable literature of core excitation spectroscopic studies of small and medium size molecules in the gas phase [2], there have been relatively few studies directly targeted at using gas phase species to model polymer components. Among these are papers dealing with Inner Shell Electron Energy Loss Spectroscopy (ISEELS) studies of small molecule modeling of poly(ethylene terephthalate) and its isomers [28,53,54], polyurethanes [22,23], conducting polymers [55,56], and Langmuir–Blodgett chains on surfaces [57–59]. In several of these cases the gas phase spectra were helpful in interpreting aspects of the polymer spectra [22,23,56], and led to useful insights as to how to use the NEXAFS spectra for analytical purposes [54].

As microanalytical tools based on inner shell

excitation continue to improve and the problems addressed become more complex, it becomes increasingly important to develop better qualitative and quantitative analysis procedures based on comparisons to spectra of compounds with known structures. If the spectra of these models contain the same spectral features at similar energy resolution to those contributing to the spectra of polymers of unknown composition, then it should be possible to develop accurate quantitative speciation procedures. Here, we illustrate the modeling aspects of our polymer microanalysis program with a selection of C 1s spectra of molecular compounds and model polymers related to the principle components of polyurethanes. Scheme 1 summarizes the structures of the molecules and polymers investigated in this work.

The apparatus and experimental procedures used for ISEELS have been described in detail elsewhere [1,60]. A final electron energy of 2.5 keV ensures that the spectra are dominated by electric dipole transitions and thus are very close to the corresponding NEXAFS spectra. The energy resolution was typically 0.7 eV fwhm, with the sharp near edge region recorded with ~0.55 eV fwhm resolution. The compounds were obtained commercially (ethyl *N*-phenyl urethane (**2**) – Eastern Chemical; *N,N′*-diphenyl urea (**1**) – Aldrich) or synthesized (2,4-toluene di(methyl carbamate) (**3**), and 4,4′ methylene bis(ethyl *N*-phenyl carbamate) (**4**)). The spectra of most materials were obtained by placing ~0.1 g in a metal tube directly attached to the collision cell. In some cases heating was required to achieve an adequate vapor density. The energy scale was calibrated by recording simultaneously the spectrum of the unknown and that of a suitable reference compound, typically CO, or CO_2 for C 1s studies [61].

Fig. 6 presents the C 1s spectra of gaseous *N,N′*-diphenyl urea (**1**), ethyl *N*-phenyl carbamate (**2**),

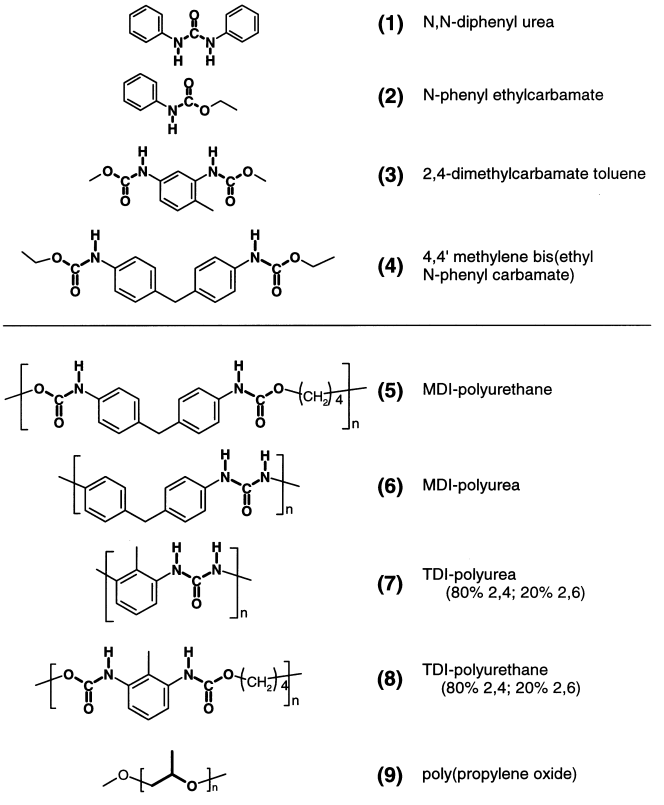

Scheme 1. Structures of molecules and model polymers related to polyurethane components that were studied in this work. The numbers are used to identify these species in the text and figures.

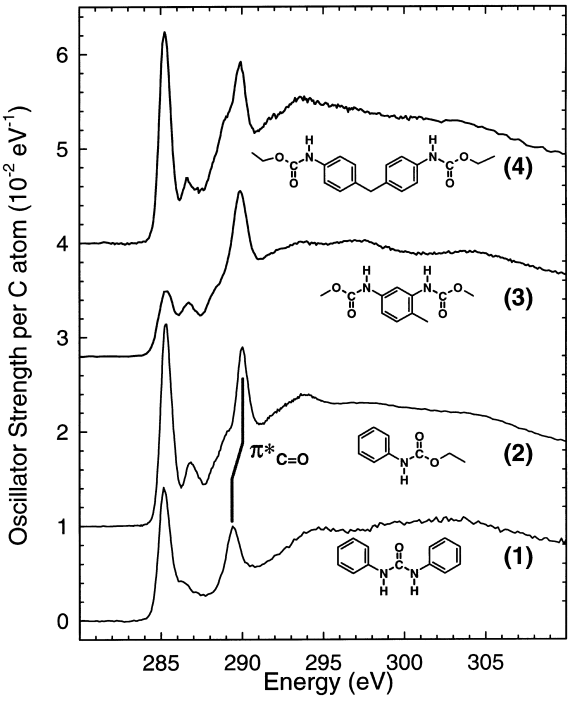

Fig. 6. Inner shell electron energy loss (ISEELS) C 1s spectra of *N,N′*-diphenyl urea (**1**), ethyl *N*-phenyl carbamate (**2**), 2,4-toluene di(methyl carbamate) (**3**) and 4,4′ methylene bis(ethyl *N*-phenyl carbamate) (**4**). In each case the as-recorded signal has been background subtracted and converted to oscillator strength per carbon atom scale. A kinematic correction has been applied to the ISEELS data to convert dipole regime electron scattering to oscillator strengths. Vertical offsets are used for clarity.

2,4-dimethylcarbamate toluene (called TDI-urethane for convenience) (**3**), and 4,4′ methylene bis(ethyl *N*-phenyl carbamate) (called MDI-urethane) (**4**). Energies and proposed assignments of the spectral features are listed in Table 1. The sharp features in these spectra are associated with transitions from the ground state to an excited state in which an electron has been promoted from a C 1s core orbital to an energy level that is unoccupied in the ground state. Although all such states rapidly decay to valence ionized states, it is meaningful to consider those features below the C 1s ionization threshold (~290 eV in the free molecules) as quasi-discrete states and those at higher energies, as short lived resonances in the C 1s ionization continuum.

While the spectra of all four species (**1–4**) are dominated by the strong C 1s→$\pi^*_{C=C}$ and C 1s→$\pi^*_{C=O}$ features around 285 and 290 eV, there are significant differences in detail which allows clear distinction of the urea and urethane functional groups, as well as between the TDI- and MDI-based materials [60]. In particular, relative to the MDI species, the TDI species has relatively weaker $\pi^*_{C=C}$ signals at 285 and 287 eV, since it has only one phenyl ring per two C=O groups, in contrast to MDI, which has one phenyl ring per C=O group. Thus the MDI-urethane (**4**) has a $\pi^*_{C=C}/\pi^*_{C=O}$ intensity ratio similar to that in (**2**). Perhaps the most significant difference is that the $\pi^*_{C=O}$ peak in urea is 0.5 eV lower in energy than the $\pi^*_{C=O}$ peak in urethanes [24]. In Fig. 6 it appears that the $\pi^*_{C=O}$ feature of urea is weaker than that in the urethane species. The urea $\pi^*_{C=O}$ peak is slightly broader, and its intensity is reduced, although not as much as suggested by the peak intensity since the urethane $\pi^*_{C=O}$ peak is 'artificially enhanced' because it sits on a back-

Table 1
Energies (±0.1 eV) and proposed assignment of features in the C 1s spectra of molecular models for MDI- and TDI-urea and urethanes

	Energy (eV)				Assignment (final orbital)			
#	**1**	**2**	**3**	**4**	C–H	C–R	aliph	C=O
1	285.14[a]	285.29[a]	285.3[a]	285.22[a]	1π*			
2	286.4	286.8	286.7	286.6		1π*		
3	–	288.1	288.1	288.2	2π*		σ^*_{C-H}	
4	–	288.9	–	288.8			σ^*_{C-H}	
5	289.45	290.0	289.9	289.9				$\pi^*_{C=O}$
6	295	294	294	294	σ^*_{C-C}	σ^*_{C-C}		
7	–	298	297	–			σ^*_{C-C}	
8	303	304	304	303	σ^*_{C-C}	σ^*_{C-C}		$\sigma^*_{C=O}$

[a] Calibration: gas: (**1**) −2.26(8) eV; (**2**) −2.11(7) eV; (**3**) −2.1(1) eV; (**4**) −2.18(6) eV relative to π* transition in CO (287.40) [61].

ground from the σ^*_{C-C} feature of the aliphatic ethyl group contained in (**2**) but not in (**1**).

3.2. Ab initio calculations of polymer model spectra

To aid the spectral assignments ab initio calculations have been performed on the C 1s excitation spectra of *N,N′*-diphenyl urea (**1**) and ethyl *N*-phenyl carbamate (**2**). These molecular species represent the local atomic and the delocalized electronic environment of the urea and carbamate groups in polyurethanes. Lower quality semi-empirical extended Hückel calculations of similar species have been reported previously [22]. Although qualitatively similar results are obtained, the higher accuracy of the ab initio methodology gives greater confidence in our spectral interpretation and better illustrates our current approach to the use of quantum chemical calculations to assist X-ray spectromicroscopy of polymers.

Calculations of the core excitation transitions were carried out using Kosugi's GSCF3 package [16,17]. Since the electronic relaxation of the core excited states induces significant alterations in the electronic structure, high level calculations are necessary in order to reliably assign inner shell spectra [62,63]. These calculations are based on the Improved Virtual Orbital approximation (IVO) which explicitly takes into account the core hole in the Hartree–Fock approximation and are highly optimized for calculation of core excited states [64]. The difference in the total energy between the core ionized and ground states energies gives the core ionization potential (IP) with a typical accuracy of $\approx$1 eV.

Optimized (minimum total energy) molecular geometries for ethyl *N*-phenyl carbamate (**2**) and *N,N′*-diphenyl urea (**1**) were determined using the program GAMESS [65] with a 4–21 G level basis. For the GSCF3 calculations, a Huzinaga [66] basis set is employed: (621/41) contracted Gaussian type functions were used on the heavy atoms (C, N and O); (41) on H; and a higher quality basis set (411121/3111/*) on the heavy atom onto which the core hole is placed. A separate calculation is performed for each symmetry inequivalent core excited atom of interest. Simulated spectra are generated from the calculational results using a Gaussian line shape for each calculated excitation. The width of these Gaussians is 0.3 eV for orbitals of eigenvalue (ϵ) $-15<\epsilon<0$; 1.2 eV for $0<\epsilon<4$; and 4.0 for $\epsilon>4.0$ eV. These values correspond to the experimental resolution for discrete transitions, and an attempt to track the approximate width of the continuum resonances which are lifetime broadened due to their rapid decay into the direct C 1s ionisation continuum. The simulated spectra are set to an approximate experimental scale by setting the zero of the calculated term value scale ($\epsilon=0$) to the calculated (ΔSCF) ionisation potential. Comparison to the experimental spectra indicate the absolute error is ~2.1 eV for each species.

The results of the ab initio calculations of (**1**) and (**2**) are presented as simulated spectra in Fig. 7. The calculations nicely reproduce the dominant spectral features, in particular the C 1s(C–H)$\rightarrow 1\pi^*_{C=C}$, C 1s(C–R)$\rightarrow 1\pi^*_{C=C}$, and C 1s(C=O)$\rightarrow\pi^*_{C=O}$ transitions. They also reproduce the large, characteristic change in the relative intensity of the $1\pi^*_{C=C}$ and $\pi^*_{C=O}$ transitions between ureas and carbamates. In addition to giving detailed insight into the origin of all the low-lying spectral features, comparison of the results for (**1**) and (**2**) indicates that the $\pi^*_{C=O}$ peak of the urea occurs ~0.4 eV below the $\pi^*_{C=O}$ peak of the urethane species, consistent with the experimental observation. The shift in the $\pi^*_{C=O}$ peak between urea and urethane is the basis for the quantitative analysis of these functional moieties, described in Section 4.

3.3. Polymer model studies by NEXAFS spectroscopy

Polymer models for important functional groups of polyurethanes (MDI-polyurea (**6**), TDI-polyurea (**7**), MDI-polyurethane (**5**), TDI-polyurethane (**8**) and polyether) were custom synthesized or were obtained from previous studies [24,67]. The polyurethane polymers used as the test targets for quantitative analysis were prepared using conventional methodologies [21] from mixtures of a poly(propylene oxide) rich polyether-polyol, toluene diisocyanate (TDI) (80% 2,4 TDI, 20% 2,6 TDI isomers), monoethylene glycol (MEG) and water according to formulations documented as a footnote to Table 2. Varying amounts of water, polyol and MEG were

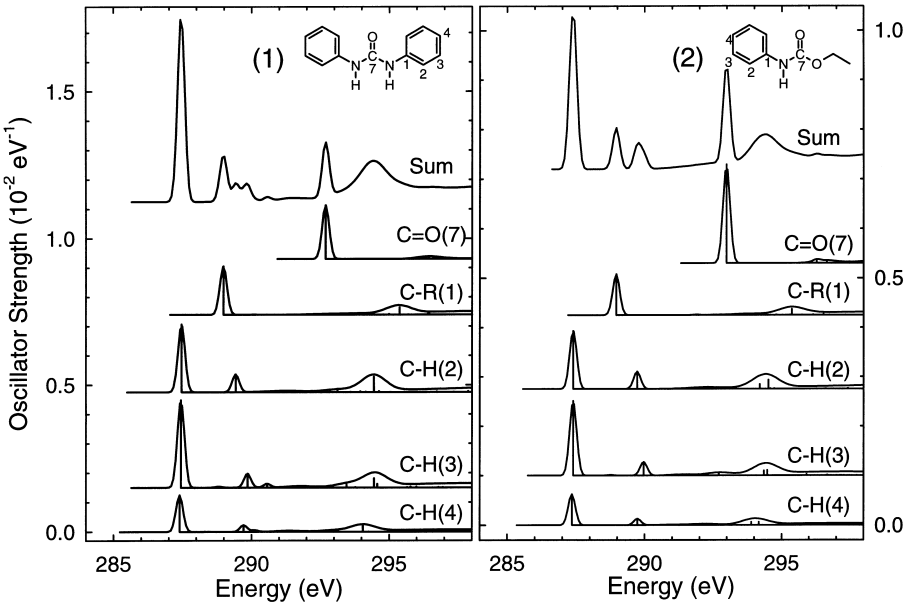

Fig. 7. Simulated C 1s spectra of *N,N′*-diphenyl urea (**1**) and ethyl *N*-phenyl carbamate (**2**) based on the results of GSCF3 calculations. The intensity of each unique carbon site is indicated, along with the appropriately weighted sum. The details of the calculations and the construction of the simulated spectra are presented in the text.

used to give a systematic change in relative amounts of urea and urethane. The synthesis was carried out without silicone surfactant in a compression mold to form a solid plaque.

C 1s NEXAFS spectra of model and test polymers were recorded with the Stony Brook STXM at beamline X1A at the NSLS [10] or the BL7.0.1 STXM at the Advanced Light Source (ALS) [11,12]. The energy resolution was typically 0.2 eV fwhm (NSLS) or 0.1 eV fwhm (ALS). Thin sections of model polymers and the polymer plaques used for analytical testing (codes: **258**, **259**, **260**) were prepared using a Reichert–Jung (now Leica) microtome with cryo-attachment at −120°C. Samples were transferred dry to unsupported copper grids with an eyelash. For homogeneous polymer samples, the X-ray beam was defocused to a 5–15 μm diameter 'donut' (the shape of a defocused zone plate beam) in order to reduce the rate of beam damage by distributing the X-ray dose over a suitably large volume of sample [28]. The analytical test samples showed some phase segregation at the submicron scale, but a sufficiently large defocus of the X-ray beam was used to average over that morphology. Energy scales were calibrated by adding CO_2 gas to the He purge in the microscope and recording the transmission spectrum of the mixture of the polymer and CO_2 gas [10]. The energies of the $CO_2 \rightarrow$Rydberg transitions from the high-resolution NEXAFS spectra of Ma et al. [68] were used to calibrate these spectra.

Fig. 8 presents the C 1s spectra of the MDI-polyurea (**6**), MDI-polyurethane (**5**), TDI-polyurea (**7**) and TDI-polyurethane (**8**) based model polymers. The energies and detailed spectral assignments have been presented and discussed elsewhere [24]. While many of the spectral features are the same as those in the molecular compounds (Fig. 6), there are also additional contributions from the polyether linkages used to make the polymer from the isocyanate monomer. In addition, all spectral features are much better resolved on account of the better spectral resolution of the NEXAFS spectrometer ($<$0.2 eV) relative to that of ISEELS ($\sim$0.6 eV). Aside from this, there is good agreement between the polymer spectra and the spectra of the molecular models

Table 2
Quantitative analysis[a] of model TDI-based polyurethane polymers

Species	Polyether			Urea			Carbamate			Quality of fit (r^2)		Standard error	
	Pred.[b]	ALS	NSLS	Pred.[b]	ALS	NSLS	Pred.[b]	ALS	NSLS	ALS	NSLS	ALS	NSLS
(a) % of Carbon-atoms of indicated component[a]													
258	70.6	66	70	25.5	28	26	3.9	6	4	0.9996	0.9996	0.0084	0.0067
259	78.2	72	75	14.5	18	17	8.0	10	8	0.9995	0.9995	0.0091	0.0078
260	77.3	70	75	8.3	13	13	16.7	17	11	0.9994	0.9997	0.0097	0.0065

Species	Polyether			Urea			Carbamate		
	Pred.[b]	ALS	NSLS	Pred.[b]	ALS	NSLS	Pred.[b]	ALS	NSLS
(b) mol% of formula units of indicated component[c]									
258	86.7	84	86	11.8	12	12	1.6	3	2
259	90.6	88	89	6.3	8	8	3.1	4	3
260	89.9	87	90	3.6	6	4	6.5	7	6

[a] Derived by a least-squares fit of the C 1s NEXAFS of the polymer to weighted sums of three model spectra. The reference signals used are the orthogonal chemical component from polyether (**E**), TDI-urea (**U**) and TDI-urethane (**C**), each on a per-carbon atom oscillator strength intensity scale – see Fig. 9. The least squares fit was performed over the energy ranges of 282–286 and 289–291 eV. These regions were selected to give maximum sensitivity to the chemical differentiation of the three components while at the same time making the procedure less sensitive to systematic errors (model generation, background subtraction and continuum normalization procedures). Concentrations have been rounded and may not add to 100.

[b] The predictions are based on the polymer formulations, expressed in mass of each reagent (arbitrary mass units). A constant amount of the catalyst DABCO 33-LV (0.6 parts) was used. The polyol is 5000 MW, trifunctional and predominantly composed of poly(propylene oxide). MEG (ethylene glycol) is a chain extender used to control the carbamate concentration.

	Polyol	TDI	Water	MEG	(arbitary mass units)
258	100	45.45	4	0	
259	100	29.86	2	1.51	
260	100	31	1.12	4.96	

The carbon atom percentages (% urea, % carbamate, % polyol) are derived from these formulations, given the molecular weight and functionality of each component and their reaction chemistry. These calculations are based on the standard polyurethane calculations of Herrington [21] except they have been extended here to the 'carbon atom concentration' which are the natural unit for NEXAFS analysis. The urea concentration is driven by the presence of water, while the carbamate concentration is driven by the presence of –OH groups in polyol and MEG.

[c] The carbon-atom-% numbers were converted to relative amounts of the repeat units (mol%) by mol%(i) = 100*{C-atom%(i))/n(i)}/{Σ_i C-atom%(i))/n(i)) where n(i) is the number of carbon atoms per repeat unit: i.e. 3, 8 and 9 for ether, urea and urethane based on the structures given in Scheme 1.

shown in Fig. 6. In particular the urea $\pi^*_{C=O}$ transitions are systematically broader, and weaker than the urethane $\pi^*_{C=O}$ transitions.

4. Quantitative chemical analysis of polyurethane polymers

The experimental and computational studies of small molecule and polymer models outlined in the previous section provides the basis for quantitative speciation of the principle components of complex polyurethane materials (urea and urethane (carbamate) linkages and the polyether copolymer). The quantitation procedure outlined in this section is based on a least squares optimization of the analyte polymer spectra to weighted sums of component spectra. This approach complements analytical methods based on singular value decomposition techniques [47]. In order to explore the quantitative

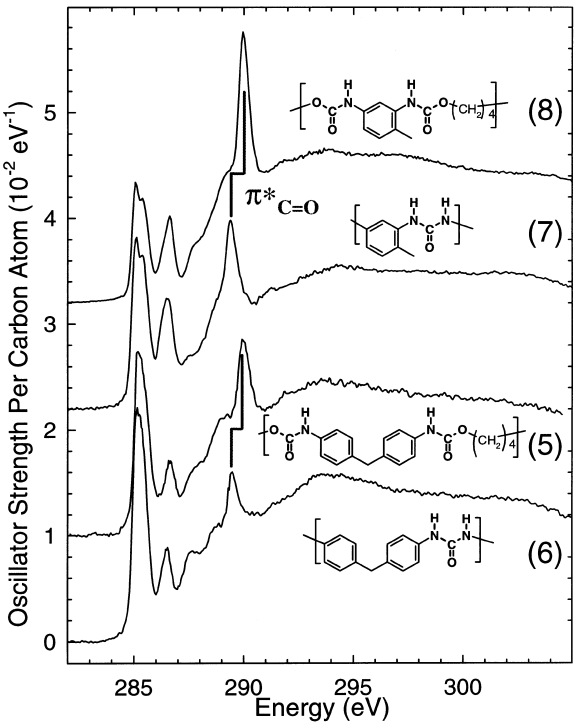

Fig. 8. NEXAFS C 1s spectra of MDI-polyurea (**6**), MDI-polyurethane (**5**), TDI-polyurea (**7**) and TDI-polyurethane (**8**). The TDI monomer used was an 80% 2,4 and 20% 2,6 isomeric mixture. In each case the as-recorded signal has been background subtracted and converted to oscillator strength per carbon atom scale (vertical offsets are used for clarity).

analysis capabilities of NEXAFS spectroscopy (and ultimately spectromicroscopy), we have performed quantitative analysis of three test polyurethane polymers (**258**, **259**, **260**) in which a controlled variation of the urea and urethane content was achieved by careful adjustment of the water content in the formulation (see Table 2). These test polymers are well suited to verify the quantitation capability of NEXAFS since a reliable estimate of ether, urea and urethane content could be made a priori from the formulation (see footnote b of Table 2 for the details).

For accurate quantitation, well-characterized NEXAFS spectra of carefully chosen models of the polymer components is required. For a blend of two or more homopolymers (i.e. polystyrene/poly(methyl methacrylate)), the analytical models can simply be the individual homopolymers. For quantitation of components in a random block copolymer (i.e. styrene acrylonitrile), the spectra of the homopolymers (polystyrene and polyacrylonitrile) can be used as component models if the polymer and monomer spectra are additive. Polyurethane polymers are complex and care must be taken in the choice of analytical models. Polyurethane polymers consist of three primary components: urea linkages (**U**), urethane or carbamate linkages (**C**) and ether linkages (**E**). Scheme 2 presents representative polyurethane structures with these units (**U**, **C**, **E**) indicated in bold. For quantitative analysis, we have produced polymer spectral standards to model these components. It is important to identify such component structures in such a way that they are orthogonal and they have a clearly defined stoichiometry. NEXAFS spectroscopy is sensitive to the relative carbon atom concentration for the different components, so the stoichiometry is needed to convert the results from the spectroscopic analysis (which we express in terms of '% of C atoms in a given unit') into more conventional wt.% or functional group concentrations.

We have adapted the C 1s spectra of TDI-polyurea (**7**), TDI-polyurethane (**8**), and poly(propylene oxide) (**9**) model polymers (presented and discussed in greater detail elsewhere [24]) to prepare standard spectra for quantitative analysis. Fig. 9 presents the

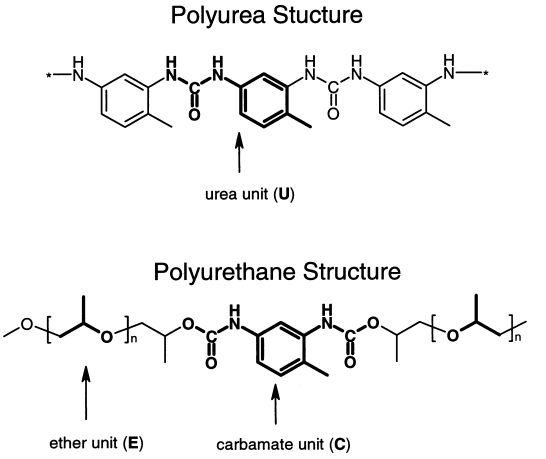

Scheme 2. Representative structures of the urea (**U**), carbamate (urethane) (**C**) and poly(propylene oxide) polyether (**E**) units upon which quantitation is based for the test polyurethanes **258**, **259** and **260**.

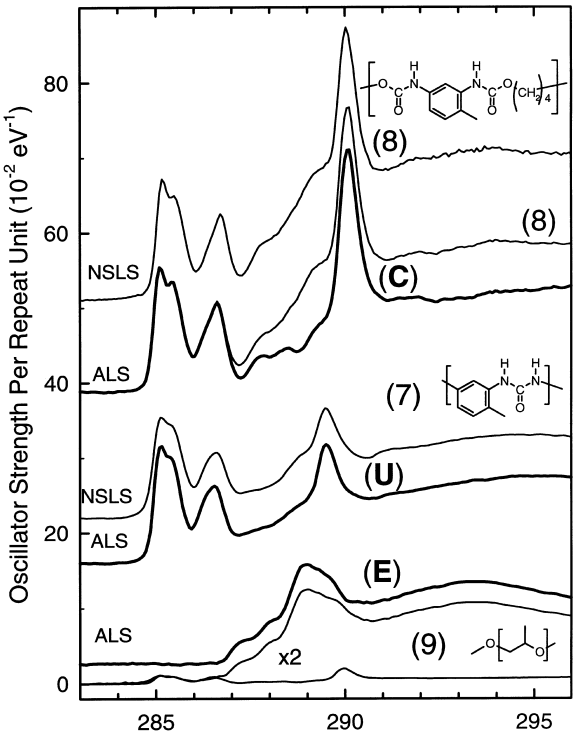

Fig. 9. Plot of the C 1s NEXAFS spectra of TDI-polyurethane (**8**), TDI-polyurea (**7**) and T3000, a polyether rich polyurethane, (**9**) which are used to derive the analytical reference standards for quantitative analysis. These spectra are presented on oscillator strength per repeat unit normalization scale. The curves labeled NSLS were recorded with the Stony Brook STXM at X-1A, all other spectra were recorded with the ALS BL 7.0 STXM. From these experimental spectra, analytical reference standards for ether (**E**), carbamate (**C**) and urea (**U**) have been derived by the subtraction of a small component of aromatic signal (as explicitly indicated for the ether signal) or aliphatic signal (in the case of carbamate) in order to isolate the pure spectral signature of the aromatic urea, aromatic urethane, and the saturated polyether.

C 1s spectra of the TDI-polyurethane (**8**), TDI-polyurea (**7**) and the poly(propylene oxide) polyether-polyol (**9**) models. The as-recorded spectra from ALS (and NSLS, for the urea and urethane species) are indicated. The repeat unit structure of the TDI-polyurea (**7**) is identical to the urea model structure (**U**) so its spectrum can be used directly as the analytical model. The polyol model (**9**) contained a small fraction of an aromatic polyurethane signal. The spectrum of the polyol analytical model (**E**) was isolated by subtracting a small urethane signal as indicated in Fig. 9. The structure of the TDI-polyurethane model (**8**) differs slightly from the carbamate model structure (**C**) due to the presence of a butane chain (from the reaction of TDI with butane diol). In order to prepare the carbamate analytical model spectrum (**C**), we approximately removed this component by subtracting a stoichimetrically weighted spectrum of poly(propylene oxide) (**9**). The spectroscopic signature of poly(propylene oxide) is expected to be close to the butane fragment present in (**8**). The original TDI-urethane spectrum (**8**) and the resulting carbamate analytical model spectrum (**C**) are presented in Fig. 9.

Fig. 10 plots the C 1s spectra of the three test polymers (codes **258**, **259**, **260**), along with the best quality fits to data recorded at the ALS BL 7.0 STXM (left panel) and at the X1A STXM at NSLS (right panel). An earlier analysis of NSLS spectra of similar statistical quality but slightly lower energy resolution has been presented elsewhere [69]. The model reference spectra (**C**, **U** and **E**) used in each analysis were those recorded with the same instrument in order to avoid artifacts associated with differences in the energy resolution.

As with all data presented in this work, the spectra of the test polymers (**258**, **259**, **260**) and the stripped spectra of the individual analytical components (**C**, **U**, **E**) were background subtracted and normalized in the far continuum on an oscillator strength per atom basis. The **C**, **U** and **E** composition of **258**, **259** and **260** was determined by a linear least squares fit over the energy range 282–286 and 289–291 eV. This choice of energy range restricts the least-squares fit to the energy region that is most sensitive to the chemical differences and where our models are most representative of the polymer chemistry. The relative aromatic fraction is determined through the C 1s(C–H)$\rightarrow\pi^*_{C=C}$ transitions of the phenyl ring in the 284–286 eV range. Simultaneously, the urea, carbamate and ether composition is determined by fitting the the 289–291 eV energy range where the adjacent urea and carbamate C 1s(C=O)$\rightarrow\pi^*_{C=O}$ transitions are superimposed on the broad ether C 1s$\rightarrow\sigma^*_{C-O}$ transitions. In the ALS data, differences between the **258**, **259** and **260** data (points) and the fits (solid lines) are most evident in the 286–289 eV region which was excluded from the least squares fit. We believe that shortcomings in the model spectra are responsible for these differences. For example use of

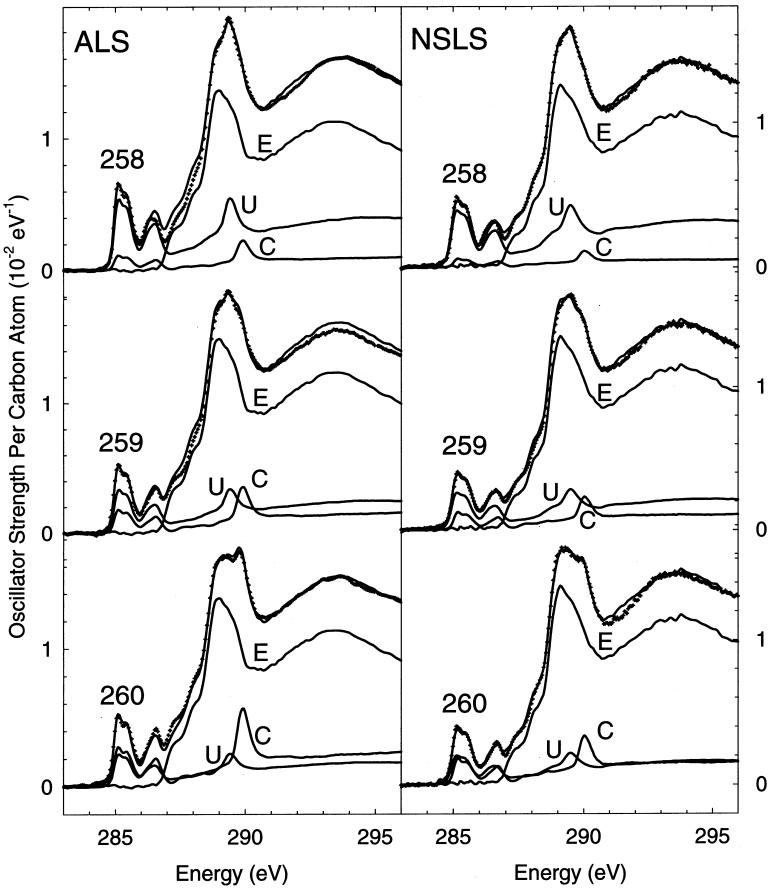

Fig. 10. Quantitative analysis of C 1s NEXAFS spectra of three different model polyurethane polymers of varying urea and urethane content. The polyurethane data is indicated by filled circle symbols, the best fit by the thicker solid line, and the amounts of the individual polyether (**E**=ether), TDI-polyurea (**U**=urea), and TDI-polyurethane (**C**=carbamate) component spectra required to construct that best fit are indicated by the thin solid lines. Vertical offsets are used for clarity.

the polyether signal to correct for the butane component of the TDI-polyurethane model (**8**) will misrepresent the urethane signal in the 286–289 eV region.

The results of the NEXAFS analysis from both ALS and NSLS data sets are compared to the composition predicted from the formulation chemistry in Table 2. The compositions are expressed in percent atom-type (the natural unit for the NEXAFS analysis, given the use of per-atom continuum normalization) and in more conventional formula unit percentages. Except for a few values for the urea and urethane composition of the test polymers with high urethane content (**260**), the NEXAFS determined composition and that predicted from the formulation agree within 20%. The quality of the match between data and optimized model (Fig. 10) demonstrates that C 1s NEXAFS spectra, when analyzed using spectra of appropriate models recorded with the same experimental conditions, can determine chemical composition at the ~10 mol% level, with 10–20% accuracy. This is a remarkably good level of quantitation given the relatively small spectral differences which are the basis for this quantitative chemical analysis (mainly the shift of ~0.5 eV between the urea and urethane $\pi^*_{C=O}$ signals around 290 eV), and the extensive overlap of these key features with the broad underlying σ^* resonances. Good energy res-

olution (<0.2 eV, preferably <0.1 eV) is a critical factor in being able to track the subtle changes in the line shapes in the 289–291 eV range which provide the sensitivity to quantitative composition. Energy scale stability is also important, as model and analyte spectra recorded at different times must be placed onto a common energy scale for this analysis. Another important factor is confidence in the absolute spectral shape for both the models and the analyte materials. The relative intensity of spectroscopic features can be affected by changes in energy resolution, linear dichroism in oriented samples, higher-order X-ray photons and detector dark noise.

While the spectra of these test polyurethanes (**258**, **259**, **260**) were acquired from relatively large areas (a few μm^2, using a defocused probe to avoid beam damage), the ultimate goal of this quantitation methodology is functional group analysis of polymers at the state-of-the-art spatial resolution of STXM (50 nm). Examples of this type of quantitative compositional analysis, carried out on spectra recorded in point mode using a fully focussed 50 nm probe, or extracted from image stack sequences [32], are being presented elsewhere, for both the polyurethane sample whose image is presented in Fig. 2 [19], and for polyurethanes with various copolymer polyol components. [20]

5. Summary

We have presented a brief overview of NEXAFS microscopy applications in polymer science and exemplified the power of NEXAFS microscopy by describing the characterization of PET/Vectra™ blends. In addition, we provided a detailed description of how NEXAFS microscopy can be used to identify polyurethane polymer components and make a quantitative analysis of these chemical components. In particular, the spectra of a number of gas and solid molecular models for the principle functional group components of polyurethane polymers have been presented and analyzed. These spectra were found to be in good agreement with the spectral features associated with the non-polyether parts of model polyurethane polymers containing the same functional groups. The spectral shape in the C $1s \rightarrow \pi^*_{C=O}$ region was shown to be a sensitive probe of the relative amounts of urea and urethane structural elements. The use of model polymer spectra for polymer compositional quantitation was demonstrated. The present results indicate that C 1s NEXAFS spectromicroscopy can determine the chemical composition of even complex polymers such as polyurethanes at the ~10 mol% level, with 10–20% accuracy, when analyzed using spectra of appropriate models recorded with the same experimental conditions.

Acknowledgements

We thank M. Adams and D. Gier (Dow Chemical) for synthesis of molecular and polymer model compounds, and G. Young (Dow Chemical) for expert preparation of the polymer thin sections. Data was recorded using the Stony Brook STXM at NSLS X-1A, the BL7.0 STXM at ALS, and the ISEELS spectrometer at McMaster. Financial support has been provided by research and partnership grants from NSERC (Canada). The Stony Brook STXM was developed by the groups of J. Kirz and C. Jacobsen, with support from the Office of Biological and Environmental Research, U.S. DOE under contract DE-FG02-89ER60858, and the NSF under grant DBI-9605045. The zone plates were developed by S. Spector and C. Jacobsen of Stony Brook and Don Tennant of Lucent Technologies Bell Labs, with support from the NSF under grant ECS-9510499. The ALS STXM was developed by T. Warwick (ALS), B. Tonner (UWM) and collaborators, with support from the U.S. DOE (contract DE-AC03-76SF00098). Zone plates at ALS were provided by Eric Anderson of CXRO, LBNL. H. Ade and A.P. Smith are supported by NSF Young Investigator Award (DMR-9458060).

References

[1] A.P. Hitchcock, Phys. Scr. T31 (1990) 159.
[2] A.P. Hitchcock, D.C. Mancini, J. Electr. Spectros. Relat. Phenom. 67 (1994) 1.
[3] J. Stöhr, NEXAFS Spectroscopy, Springer-Verlag, Berlin, 1992.
[4] H. Ade, Trends Polym. Sci. 5 (1997) 58.

[5] J. Kirz, C. Jacobsen, M. Howells, Q. Rev. Biophys. 28 (1995) 33.
[6] H. Ade, X. Zhang, S. Cameron, C. Costello, J. Kirz, S. Williams, Science 258 (1992) 972.
[7] H. Ade, B. Hsiao, Science 262 (1993) 1427.
[8] H. Ade, A. Smith, S. Cameron, R. Cieslinski, C. Costello, B. Hsiao, G. Mitchell, E. Rightor, Polymer 36 (1995) 1843.
[9] A.P. Smith, H. Ade, Appl. Phys. Lett. 69 (1996) 3833.
[10] H. Ade, A.P. Smith, H. Zhang, G.R. Zhuang, J. Kirz, E. Rightor, A.P. Hitchcock, J. Electron Spectrosc. Relat. Phenom. 84 (1997) 53.
[11] T. Warwick, H. Ade, S. Cerasari, J. Denlinger, K. Franck, A. Garcia, S. Hayakawa, A. Hitchcock, J. Kikuma, J. Kortright, G. Maigs, M. Moronne, S. Myneni, E. Rightor, E. Rotenberg, S. Seal, H.-J. Shin, R. Steele, T. Tyliszczak, B. Tonner, Rev. Sci. Instrum. 69 (1998) 2964.
[12] T. Warwick, H. Ade, A.P. Hitchcock, H. Padmore, E.G. Rightor, B.P. Tonner, J. Electron Spectrosc. Relat. Phenom. 84 (1997) 85.
[13] R.F. Egerton, Electron Energy Loss Spectroscopy in the Electron Microscope, Plenum Press, New York, 1986.
[14] M.M. Disco, in: M.M. Disko, C.C. Ahn, B. Fultz (Eds.), Transmission Electron Energy-Loss Spectrometry in Materials Science, TMS, 1992.
[15] H. Agren, V. Carravetta, O. Vahtras, L.G.M. Pettersson, Chem. Phys. Lett. 222 (1994) 75.
[16] N. Kosugi, K.H. Kuroda, Chem. Phys. Lett. 74 (1980) 490.
[17] N. Kosugi, Theor. Chim. Acta 72 (1987) 149.
[18] L. Triguero, L.G.M. Pettersson, H. Agren, Phys. Rev. B 58 (1998) 8097.
[19] E.G. Rightor, G.E. Mitchell, S.G. Urquhart, A.P. Smith, H. Ade, A.P. Hitchcock, in preparation.
[20] A.P. Hitchcock, T. Tyliszczak, E.G. Rightor, G.E. Mitchell, M.T. Dineen, W. Lidy, R.D. Priester, S.G. Urquhart, A.P. Smith, H. Ade, in preparation.
[21] R. Herrington, Flexible Polyurethane Foams, 2nd ed, The DOW Chemical Company, 1997.
[22] S.G. Urquhart, A.P. Hitchcock, R.D. Priester, E.G. Rightor, J. Polym. Sci. B, Polym. Phys. 33 (1995) 1603.
[23] S.G. Urquhart, A.P. Hitchcock, R.D. Leapman, R.D. Priester, E.G. Rightor, J. Polym. Sci. B, Polym. Phys 33 (1995) 1593.
[24] S.G. Urquhart, H.W. Ade, A.P. Smith, A.P. Hitchcock, E.G. Rightor, W. Lidy, J. Phys. Chem. B 103 (1999) 4603.
[25] J.C. Moreland, G.L. Wilkes, R.B. Turner, E.G. Rightor, J. Appl. Polym. Sci. 52 (1994) 1459.
[26] J.P. Armistead, G.L. Wilkes, J. Appl. Polym. Sci. 35 (1988) 601.
[27] A.P. Smith, C. Bai, H. Ade, R.J. Spontak, C.M. Balik, C.C. Koch, Macromol. Rapid Commun. 19 (1998) 557.
[28] E.G. Rightor, A.P. Hitchcock, H. Ade, R.D. Leapman, S.G. Urquhart, A.P. Smith, G.E. Mitchell, D. Fisher, H.J. Shin, T. Warwick, J. Phys. Chem. B 101 (1997) 1950.
[29] G.E. Mitchell, S.G. Urquhart, L. Wilson, M. Dineen, E.G. Rightor, A.P. Hitchcock, U. Neuhaeusler, H.W. Ade, W. Meyer-Ilse, J.T. Brown, T. Warwick, Advanced Light Source Compendium 1997, LBNL Report 41658 (1998).
[30] G.E. Mitchell, S.G. Urquhart, M. Dineen, E.G. Rightor, H. Ade, A.P. Hitchcock, W. Meyer-Ilse, L. Wilson, in preparation.
[31] S. Zhu, Y. Liu, M.H. Rafailovich, J. Sokoloc, D. Gersappe, A. Winesett, H. Ade, Nature (1999) in press
[32] C. Jacobsen, S. Wirick, G. Flynn, C. Zimba, J. Microscopy, in press.
[33] J. Maser, A. Osanna, Y. Wang, R. Fliller, C. Jacobsen, J. Kirz, S. Spector, M. Weigel, B. Winn, D. Tennant, J. Microsc., (1999) in preparation.
[34] A.P. Smith, H. Ade, R.J. Sponta, C.C. Koch, Microsc. Microanal. 4 (S-2) (1998) 142.
[35] A.P. Smith, H. Ade, R.J. Spontak, C.C. Koch, S.D. Smith, Adv. Mater., in preparation.
[36] A.P. Smith, J.H. Laurer, H.W. Ade, S.D. Smith, A. Ashraf, R. Spontak, Macromolecules 30 (1996) 663.
[37] A. Cossy-Favre, J. Diaz, Y. Liu, H. Brown, M.G. Samant, J. Stöhr, A.J. Hanna, S. Anders, T.P. Russell, Macromolecules 31 (1998) 4957.
[38] S. Anders, T. Stammler, C. Singh Bhatia, J. Stohr, W. Fong, C.-Y. Chen, D.B. Bogy, Mater. Res. Soc. Proc. 517 (1998) 415.
[39] S. Anders, T. Stammler, W. Fong, D.B. Bogy, C. Singh Bhatia, J. Stöhr, J. Vac. Sci. Technol. A, in press.
[40] A. Cossy-Favre, J. Diaz, S. Anders, H. Padmore, Y. Liu, M. Samant, J. Stohr, H. Brown, T.P. Russell, Acta Phys. Polonica A 91 (1997) 923.
[41] H. Ade, D.A. Winesett, A.P. Smith, S. Anders, T. Stammler, C. Heske, D. Slep, M.H. Rafailovich, J. Sokolov, J. Stöhr, Appl. Phys. Lett. 73 (1998) 3773.
[42] H. Ade, D.A. Winesett, A.P. Smith, S. Qu, S. Ge, S. Rafailovich, J. Sokolov, Europhs. Lett. 45 (1999) 526.
[43] A.P. Hitchcock, S.G. Urquhart, H. Ade, E.G. Rightor, W. Lidy, Microsc. Microanal. 5 (S-2) (1998) 808.
[44] H. Ade, A.P. Smith, G.R. Zhuang, B. Wood, I. Plotzker, E.G. Rightor, D.-J. Liu, S.-C. Lui, C. Sloop, Mater. Res. Soc. Symp. Proc. 437 (1996) 99.
[45] J. Kikuma, T. Warwick, H.J. Shin, J. Zhang, B.P. Tonner, J. Electron Spectrosc. Relat. Phenom. 94 (1998) 271.
[46] X. Zhang, C. Jacobsen, S. Lindaas, S. Williams, J. Vac. Sci. Technol., B 13 (1995) 1477.
[47] X. Zhang, R. Balhorn, J. Mazrimas, J. Kirz, J. Struc. Biol. 116 (1996) 335.
[48] G.D. Cody, R.E. Botto, H. Ade, S. Behal, M. Disko, S. Wirick, Energy & Fuels 9 (1995) 153.
[49] G.D. Cody, R.E. Botto, H. Ade, S. Behal, M. Disko, S. Wirick, Energy & Fuels 9 (1995) 525.
[50] G.D. Cody, H. Ade, S. Wirick, G.D. Mitchell, A. Davis, Org. Geochem. 28 (1998) 441.
[51] R.E. Botto, G.D. Cody, J. Kirz, H. Ade, S. Behal, M. Disko, Energy & Fuels 8 (1994) 151.
[52] H. Ade, in: J.A.R. Samson, D.L. Ederer (Eds.), Experimental Methods in the Physical Science, Academic Press, 1998.
[53] A.P. Hitchcock, S.G. Urquhart, E.G. Rightor, J. Phys. Chem. 96 (1992) 8736.
[54] S.G. Urquhart, A.P. Hitchcock, A.P. Smith, H. Ade, E.G. Rightor, J. Phys. Chem. B 101 (1997) 2267.
[55] J.T. Francis, A.P. Hitchcock, J. Phys. Chem. 96 (1992) 6598.

[56] A.P. Hitchcock, G. Tourillon, R. Garrett, G.P. Williams, C. Mahatsekake, C. Andrieu, J. Phys. Chem. 94 (1990) 2327.
[57] D.A. Outka, J. Stohr, J.P. Rabe, J.D. Swalen, J. Chem. Phys. 88 (1988) 4076.
[58] J. Stöhr, D.A. Outka, K. Baberscke, D. Arvanitis, J.A. Horsley, Phys. Rev. B 36 (1987) 2976.
[59] D.A. Outka, J. Stöhr, J. Chem. Phys. 88 (1988) 3539.
[60] S.G. Urquhart, Core Excitation Spectroscopy of Molecules and Polymers, Ph.D. Thesis, McMaster University, Hamilton, ON, Canada, 1997.
[61] R.N.S. Sodhi, C.E. Brion, J. Electron Spectrosc. 34 (1984) 363.
[62] N. Kosugi, J. Adachi, E. Shigemasa, A. Yagishita, J. Chem. Phys. 97 (1992) 8842.
[63] N. Kosugi, E. Shigemasa, A. Yagishita, Chem. Phys. Lett. 190 (1992) 481.
[64] W.J. Hunt, W.A.I. Goddard, Chem. Phys. Lett. 3 (1969) 414.
[65] M.W. Schmidt, K.K. Baldridge, J.A. Boatz, S.T. Elbert, M.S. Gordon, J.J. Jensen, S. Koseki, N. Matsunaga, K.A. Nguyen, S. Su, T.L. Windus, M. Dupuis, J.A. Montgomery, J. Computational Chem. 14 (1993) 1347.
[66] S. Huzinaga, J. Andzelm, M. Klobukowski, E. Radzio-Andzelm, Y. Sasaki, H. Tatewaki, Gaussian Basis Sets for Molecular Orbital Calculations, Elsevier, Amsterdam, 1984.
[67] C.P. Christenson, M.A. Hartcock, M.D. Meadows, H.L. Spell, W.L. Howard, M.W. Creswick, R.E. Guerra, R.B. Turner, J. Polym. Sci.: Part B: Polym. Phys. 24 (1986) 1401.
[68] Y. Ma, C.T. Chen, G. Meigs, K. Randall, F. Sette, Phys. Rev. A 44 (1991) 1848.
[69] A.P. Hitchcock, S.G. Urquhart, E.G. Rightor, W. Lidy, H. Ade, A.P. Smith, T. Warwick, Microsc. Microanal. 3 (S-2) (1997) 909.